

# Hopfield Neural Network for Plasma Image Reconstruction in Application to a Bolometer Camera System of LHD

Naofumi IWAMA, Noriyuki ICHIKAWA, Yohsuke HOSODA<sup>1)</sup>, Yi LIU<sup>2)</sup>, Naoki TAMURA<sup>3)</sup>, Byron J. PETERSON<sup>3)</sup>, and Artem Yu. KOSTRYUKOV<sup>4)</sup>

*School of Informatics, Daido Institute of Technology, Nagoya 457-8530, Japan*

<sup>1)</sup>*Department of Information Science, Fukui University, Fukui-shi 910, Japan*

<sup>2)</sup>*South-Western Institute of Physics, Chengdu 610041, China*

<sup>3)</sup>*National Institute of Fusion Science, Toki 509-5292, Japan*

<sup>4)</sup>*St. Petersburg Technical University, St. Petersburg, Russia*

(Received: 30 August 2008 / Accepted: 1 April 2009)

The Hopfield neural network has been studied for improving the sparse-data tomography of plasma. By using a differentiation operator and an appropriate nonlinear activation function in the neural model, the network gives a useful result of well reconstructing smooth and positive-valued image profiles. Data structure formats in computer coding for sparse matrices are useful for accelerating the neuron state updating. Study is also made for optimizing the regularization parameter that is involved in interconnecting weights. Concerning a bolometer camera system of LHD, the results of data analysis and numerical simulation are presented in comparison with those of the Tikhonov-Phillips method and the maximum entropy method using a fast Newton algorithm.

Keywords: Hopfield neural network, plasma imaging, sparse-data tomography, bolometer camera, LHD

## 1. Introduction

The Hopfield neural network [1,2] can be a tool of regularizing the ill-conditioned least-squares solutions of linear equations in formulation of Tikhonov-Phillips (TP) type, if necessary, with an additional nonlinear constraint of positive value of the solutions, and can be applied to the tomographic image reconstruction of plasma. In this paper, neural model design is studied for the purpose of fast and stably obtaining smooth and positive-valued images and examined on the bolometer camera data of the Large Helical Device (LHD) [3-6]. The result is compared with those of the TP method [7] and the maximum entropy method (MEM) with a fast Newton algorithm whose usefulness was proved for the solar flare imaging using the satellite Yohkoh hard x-ray telescope (HXT) [8,9].

In the next section, the design of the Hopfield neural network on the interconnecting weights, the biases and the activation function of neurons is described. Results of LHD bolometer data analysis and numerical simulations are presented in Sec. 3 and summarized in Sec. 4.

## 2. Hopfield Neural Network Design for Image Reconstruction

### 2.1 Dynamics of Hopfield neural network

The neural net of Hopfield type [1] is a system which consists of mutually interconnected neurons as shown in Fig. 1. The Hopfield type means that this system of  $K$  neurons has a dynamical behavior expressed by a set of

author's e-mail: n-iwama@daido-it.ac.jp

differential equations

$$a_i \frac{du_i}{dt} = \sum_{j=1}^K w_{ij} f_j + \theta_i \quad (i = 1, 2, \dots, K), \quad (1)$$

where  $u_i$  and  $f_i$  are the internal state and the output of the  $i$ -th neuron, respectively, which are related with an activation function  $f_i = \phi(u_i)$ , that is, the input-output relation in each neuron. And  $w_{ij}$  is a constant representing the interconnecting weight from the  $j$ -th to  $i$ -th neuron, and  $\theta_i$  is the bias of the  $i$ -th neuron which is also given a constant;  $a_i$ 's ( $>0$ ) are relaxation constants. Through the function  $f_i = \phi(u_i)$ , Eq. (1) is essentially an equation system for the internal states  $u_i$  ( $i=1, 2, \dots, K$ ).

With this definition, the neural system is shown to have a quantity

$$E = -\frac{1}{2} \sum_{i=1}^K \sum_{j=1}^K w_{ij} f_i f_j - \sum_{i=1}^K \theta_i f_i, \quad (2)$$

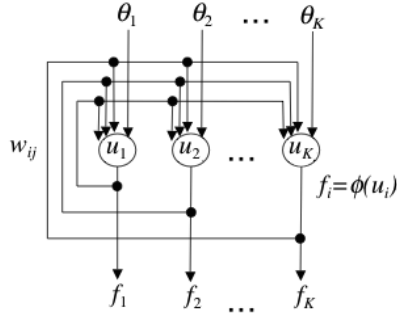
to be termed an energy function since it always tends to decrease. In fact, from Eqs. (1) and (2) one gets a relation

$$\frac{dE}{dt} = \sum_{i=1}^K a_i \frac{d\phi(u_i)}{du_i} \left( \frac{du_i}{dt} \right)^2,$$

provided that the weights are symmetric such as  $w_{ij} = w_{ji}$  for all  $i$  and  $j$ . Consequently, if  $\phi(u_i)$  is a monotonically increasing function, one always has  $dE/dt \leq 0$ .

By adopting matrix notations, Eqs. (1) and (2) are written briefly as

$$\frac{dv}{dt} = Wf + \theta, \quad E = -\frac{1}{2} f^T Wf - \theta^T f, \quad (3)$$


 Fig.1 Hopfield model with  $K$  neurons

where  $\mathbf{v}$ ,  $\mathbf{f}$  and  $\boldsymbol{\theta}$  are  $K$ -dimensional column vectors with components of  $a_i u_i, f_i$  and  $\theta_i$ , respectively, and  $W$  is a  $K$ -dim. square matrix with elements  $w_{ij}$ .

## 2.2 Hopfield model for linear inverse problems

With the above neural model, one can solve the optimization problems of TP type with a nonlinear modification. Let us consider the inverse problem expressed by an ill-conditioned linear equation  $H\mathbf{f}=\mathbf{g}$  with a  $K$ -dim. column vector  $\mathbf{f}$  and an  $M$ -dim. one  $\mathbf{g}$ . In the case of tomography,  $\mathbf{f}$  is an image vector composed of the  $K$  unknown pixel values that should be determined from a data vector  $\mathbf{g}$  composed of  $M$  detector outputs, and  $H$  is a projection matrix related to the geometry of the lines of sight.

A standard approach to the well-regularized solution is to minimize a penalty function  $P(\mathbf{f})$  under the constraint that the mean square error  $(1/M)\|H\mathbf{f}-\mathbf{g}\|^2$  should be equal to a constant. Then, the problem is reduced to minimizing the Lagrange function

$$\Lambda(\mathbf{f}) = \gamma P(\mathbf{f}) + (1/M)\|H\mathbf{f} - \mathbf{g}\|^2 \quad (4)$$

with a regularization parameter  $\gamma (>0)$ . With  $P(\mathbf{f})=\|C\mathbf{f}\|^2$  where  $C$  is either the identity matrix or a differentiation operator, one gets the TP solution

$$\hat{\mathbf{f}} = (H^T H + M\gamma C^T C)^{-1} H^T \mathbf{g}, \quad (5)$$

which can further be rewritten to a useful form of orthogonal series expansion by adopting the singular value decomposition of  $HC^{-1}$  [7]. This solution  $\hat{\mathbf{f}}$  is linear with  $\mathbf{g}$  and fast in computing for the variation of  $\mathbf{g}$ , but the components  $\hat{f}_i$  may take negative values.

Now, one finds a significant analogy between this Lagrange function  $\Lambda(\mathbf{f})$  and the energy function  $E$  of Hopfield model. Rewriting  $\Lambda(\mathbf{f})$  with  $P(\mathbf{f})=\|C\mathbf{f}\|^2$  as

$$\Lambda(\mathbf{f}) = \mathbf{f}^T (1/M)(H^T H + M\gamma C^T C) \mathbf{f} - (2/M)\mathbf{g}^T H\mathbf{f} + (1/M)\mathbf{g}^T \mathbf{g}$$

and neglecting the constant term  $(1/M)\mathbf{g}^T \mathbf{g}$ , we see that the above  $\Lambda(\mathbf{f})$  is reduced to  $E$  by putting

$$W = -\frac{2}{M}(H^T H + M\gamma C^T C), \quad \boldsymbol{\theta} = \frac{2}{M}H^T \mathbf{g}. \quad (6)$$

This relationship suggests that the Hopfield model

provided with this symmetric weight matrix  $W$  and this bias vector  $\boldsymbol{\theta}$  will give the minimizer  $\mathbf{f}$  of  $E$  as a result of learning, that is, in the stationary state that will be attained after iterations according to Eq. (1). It is to be noted that this minimizer is not equal to the solution of TP, but it gives the solution  $\mathbf{u}$  of the stationary state equation

$$W\mathbf{f} + \boldsymbol{\theta} = \mathbf{0} \quad \text{with } f_i = \phi(u_i) \quad (i = 1, 2, \dots, K). \quad (7)$$

Apparently, when the sigmoid function is used for  $\phi(u_i)$ , Eq. (7) is nonlinear in such a way that all the components  $f_i$ 's of the solution  $\mathbf{f}$  are hold positive-valued. When the ramp function  $\phi(u_i)=u_i$  ( $-\infty < u_i < \infty$ ) is used, the solution coincides with the solution of TP. Therefore, one can state that the minimization of  $\Lambda(\mathbf{f})$  using the Hopfield neural network will be a method of nonlinear regularization with positive-value guarantee, which is a method different from MEM employing the neg-entropy for  $P(\mathbf{f})$  in Eq. (4).

## 2.3 Numerical procedure for solution

Eq. (5) means that the TP solution is naturally obtained by inverting a preliminary solution  $H^T \mathbf{g}$  with the operator  $H^T H + M\gamma C^T C$ . Eq. (6) requires that this preliminary solution and operator of TP are given to the Hopfield model as the bias  $\boldsymbol{\theta}$  and the weight  $W$ , respectively. Updating the neuron states by Eq. (1) means that the TP inversion is replaced by the repetition of the forward calculation  $W\mathbf{f}+\boldsymbol{\theta}$  for updating the vector  $\mathbf{u}$ .

In this paper, we start with an initial system state of  $u_i^{(0)} = \phi^{-1}(f_i^{(0)})$  and execute the  $(n+1)$ th iteration based on the Euler approximation of Eq. (1), that is,

$$u_i^{(n+1)} = u_i^{(n)} + \Delta u_i, \quad \Delta u_i = \left( \sum_{j=1}^K w_{ij} f_j^{(n)} + \theta_i \right) \frac{\Delta t}{a_i} \quad (8)$$

for  $i = 1, 2, \dots, K$ . It is meaningful to note that this iteration for minimizing the function  $E$  is a modification of the steepest descent iteration which is to be carried out with

$$\Delta u_i = \left( \sum_{j=1}^K w_{ij} f_j^{(n)} + \theta_i \right) \left. \frac{d\phi_i}{du_i} \right|^{(n)} \frac{\Delta t}{a_i}.$$

Comparing with Eq. (8) and recalling Eq. (7), one can state that, when the ramp function is used for  $\phi(u_i)$ , the Hopfield iteration is reduced to the steepest descent iteration and will yield the linear solution of TP.

To get a smooth profile of plasma, we employ the Laplacian operator for  $C$ . To avoid the saturation of image values  $f_i$ , we replace the sigmoid function by the skimmer function [10]

$$\phi(u_i) = u_i + \ln[1 + \exp(-u_i)] \quad (-\infty < u_i < \infty), \quad (9)$$

which is a monotonically increasing function with a derivative of sigmoid function form  $d\phi(u_i)/du_i = [1 + \exp(-u_i)]^{-1}$ , being similar to the ramp function  $\phi(u_i) \approx u_i$  for  $u_i \gg 1$  and converging to zero as

$u_i \rightarrow -\infty$ . Also, we carry out the asynchronous updating of neuron states by Eq. (8), changing the order of  $K$  neurons every iteration using the random number. In this calculation, regarding that the matrices  $H$  and  $W$  for tomography are sparse, we omit the zero elements of these matrices beforehand in computer coding using the compressed column/row storage (CCS/CRS) formats [11]. Excluding the multiplication of zero value will accelerate the iterative calculation.

### 3. Application to Bolometer Data of LHD

#### 3.1 Observed behavior of neural network

The Hopfield method described above was applied to the signals of a bolometer camera system of LHD. As displayed in Fig. 2, the system consists of two 20-channel pinhole cameras with AXUVD silicon photodiode arrays and has been installed in a semi-tangential plane viewed with 3.5U/4-O ports of LHD [3-6]. For the number of detectors of  $M=40$  and the pixellation of the imaging region with  $K=32 \times 32$ , the matrix  $H$  was evaluated by taking into account the beam-width due to the finite detector surface and the finite receiving solid angle, which were considered also for the calibration of signals  $g$ .

The weight matrix  $W$  and the bias vector  $\theta$  are as plotted in Fig. 3. The weights to a neuron allocated at the  $i$ -th pixel are composed of three portions: 1) the negative self-feedback  $w_{ii}$ , 2) the positive feedbacks  $w_{ij}$  from four neighboring neurons, and 3) the negative feedbacks  $w_{ij}$  from all the neurons including itself that exist along the line of sight passing the  $i$ -th pixel. The first two portions arise only from the term  $M\gamma C^T C$  and will contribute to the stability of the pixel value  $f_i$  and the smoothness of profile

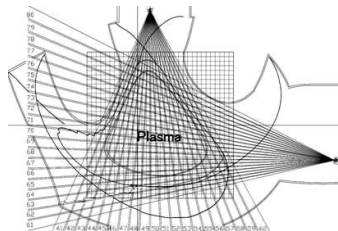


Fig. 2 View fields of two fan-beam bolometer cameras and the square imaging region in a cross section of LHD.

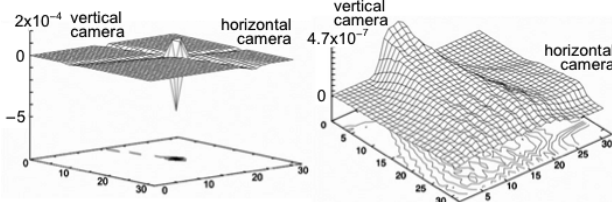


Fig. 3 (a) Weights to a neuron which is located at a pixel passed by two lines of sights:  $32 \times 32$  image-like plot of  $w_{500,j}$  as a function of  $j$  ( $=1, 2, \dots, K$ ) for  $\gamma = 1.0 \times 10^{-5}$ ; (b)  $32 \times 32$  image-like plot of the biases  $\theta_i = (2/M)(H^T g)_i$  of  $K$  neurons (LHD shot no 31721,  $t=2.00$  s).

around the  $i$ -th pixel. The third portion arises only from the term  $H^T H$  and agrees with the requirement of fitting the projection  $(Hf)_m$  to the detector output  $g_m$ . Neurons that exist outside the view fields of camera are provided only with the first two portions and isolated having liaisons with only four neighbors. Meanwhile, the bias  $\theta$  proportional to  $H^T g$  presents a preliminary image like two overlapped fan-beams which is produced by a back-projection procedure, that is, by redistributing each detector output  $g_m$  to the pixels along the  $m$ -th line of sight with the weights  $h_{mi}$ . A neuron given a larger positive bias tends to excite. Then, the obtained Hopfield model behaved as shown in Fig. 4. It is seen that, with an initial image nearly equal to zero and with a value of  $\gamma$ , the energy function  $E$  decreases monotonically and the plasma image is built up gradually as the iteration goes until  $E$  reaches an almost stationary state, where the projection  $H\hat{f}$  of the reconstructed image  $\hat{f}$  well fits the data  $g$ . The image  $\hat{f}$  is in accordance with the magnetic surface and demonstrates a gas-puff enhancement of radiation in the bottom of the imaging region. The nonzero outputs of the 21st and 40th detectors indicate the existence of plasma outside of the view field of the horizontal camera, especially, at the bottom region. And an artifact appears near the horizontal camera in a region passed by no line of sight.

This result was obtained by setting all  $a_i$ 's to  $a=10^{-2}$

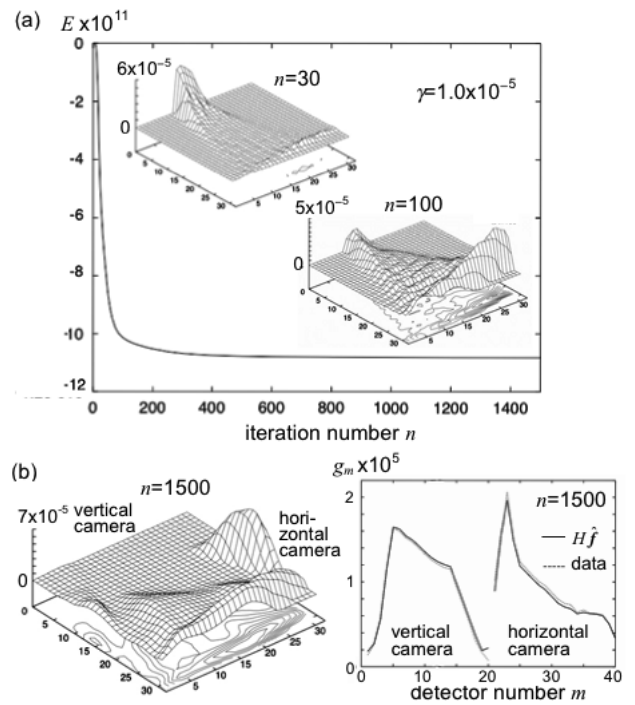


Fig. 4 Result of Hopfield method: (a) Time changes of energy function  $E$  and plasma image  $f$ ; (b) Reconstructed image  $\hat{f}$  for  $n=1500$  (left) and its projection  $(H\hat{f})_m$  and data  $g_m$  (right);  $\gamma = 1.0 \times 10^{-5}$  (LHD shot no 31721,  $t=2.00$  s). Detector number  $m$  from 1 to 40 counts up the lines of sight in Fig. 2 from the left in vertical camera and then from the bottom in horizontal camera.

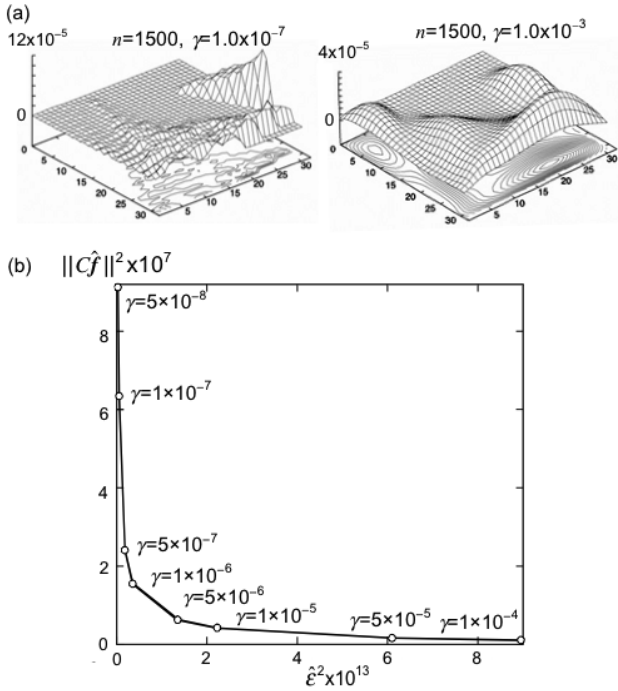


Fig. 5 (a) Change of the reconstructed image  $\hat{f}$  with  $\gamma$ , and (b) L-curve showing the dependence of  $\|C\hat{f}\|^2$  on  $\hat{\epsilon}^2$  in Hopfield analysis (LHD shot no 31721,  $t=2.00$  s).

with  $\Delta t=1$  and by choosing the scaling factor  $\rho$  of data  $\mathbf{g}$  as  $\rho = 1.0 \times 10^5$ . The factor  $\rho$  was adopted to appropriate the order of magnitude of  $g_m$  not only for a practical purpose of adequate neuron inputs but also for the purpose of accelerating the system updating; a larger value of  $\rho$  lead to a better use of the ramp-like part of the skimmer function and thus easily to faster updating as long as the Euler approximation in Eq. (8) was good enough. Contrarily, the sigmoid function required carefully arranging the values of  $\rho$  and  $a$  both for avoiding the saturation of  $f_i$  and for fast convergence. The ramp function lead to the fastest convergence to the image reconstruction very similar to that of TP. For any choices of activation function and parameter values, the CCS/CRS formats were

powerful for efficient computing. Particularly, the use of the CRS format for calculating  $Wf^{(n)}$  in the right side of Eq. (8) resulted in computing time decrease by a factor of about 1/6 for once updating the whole  $K$ -neuron system. This factor was nearly equal to the number ratio of nonzero elements in the matrix  $W$ .

Now, the image  $\hat{f}$  changes as shown in Fig. 5(a). The  $\gamma$  value in Fig. 4 was chosen practically in regarding the dependence of the attained mean square error  $\hat{\epsilon}^2 = (1/M)\|H\hat{f} - \mathbf{g}\|^2$  on  $\gamma$  and also the L-curve [12], which is a parametrized curve of  $\|C\hat{f}\|^2$  versus  $\hat{\epsilon}^2$  with the change of  $\gamma$  as plotted in Fig. 5(a). It is in the TP method that the L-curve criterion has been theoretically validated, but it is possible to calculate in the Hopfield method regardless to nonlinear modification. The obtained L-curve shows that, when  $\gamma$  is decreased,  $H\hat{f}$  approaches to  $\mathbf{g}$  with a monotonic decrease of  $\hat{\epsilon}^2$  while the image  $\hat{f}$  improves at first with a gradual increase of  $\|C\hat{f}\|^2$  and then suffers from its rapid increase reflecting the noise enhancement due to the ill-condition of the equation  $Hf = \mathbf{g}$ . On the bolometer system of LHD, simulations on numerically generated data  $\mathbf{g} = Hf_0 + \mathbf{n}$  with known images  $f_0$  and zero-mean Gaussian noises  $\mathbf{n}$  have suggested that the optimal images are obtained at the right side of the corner of L-curve, that is, for the  $\gamma$  value a little larger than the value for which the rapid decrease of  $\hat{\epsilon}^2$  ends; also, the optimal value of  $\gamma$  is smaller than the value which is selected with the Morozov condition using the known mean square value of noises.

### 3.2 Comparison with TP method and MEM and results for a variation of data

On the same bolometer data, results of analysis by the TP method and MEM are exhibited in Figs. 6 and 7. With the condition number  $\sigma_1/\sigma_{40}=607.4$  of  $HC^{-1}$  (i.e., the ratio of the maximum and minimum singular value), the TP method gave smooth profiles of emissivity which varied with  $\gamma$  as shown in the insets of Fig. 6. The generalized cross validation (GCV) [13] took a minimum for  $\gamma=1 \times 10^{-4}$ , where the linear low-pass filtering based on the singular-

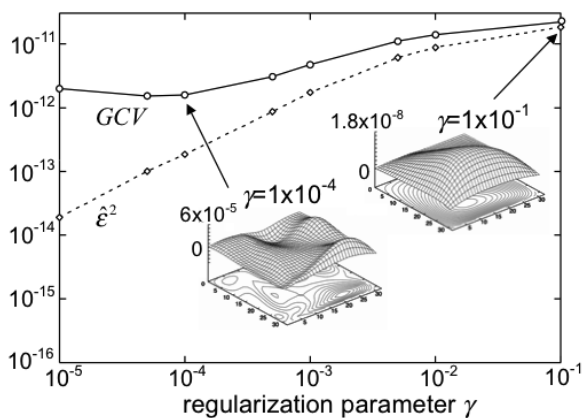


Fig. 6 Result of TP method: changes of  $GCV$ ,  $\hat{\epsilon}^2$  and  $\hat{f}$  with  $\gamma$  (LHD shot no 31721,  $t=2.00$  s).

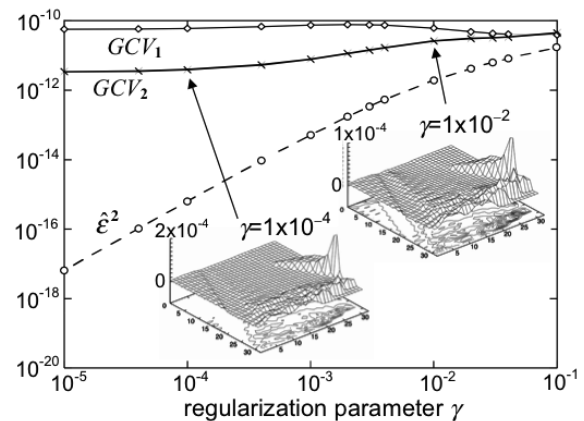


Fig. 7 Result of MEM: Changes of  $GCV_1$ ,  $GCV_2$ ,  $\hat{\epsilon}^2$  and  $\hat{f}$  with  $\gamma$  (LHD shot no 31721,  $t=2.00$  s).

vector series expansion might be optimal. The image  $\hat{f}$  so-selected took negative values in a region having no line of sight near the vertical camera. On the other hand, as shown in the insets of Fig. 7, the MEM gave rough profiles due to the weak regularization with no negative pixel value.

This result of MEM was obtained by the fast algorithm using the matrix formula of Sherman-Morrison-Woodbury (SMW) [8,9,5]. When one minimizes the function  $\Lambda(\mathbf{f})$  in Eq. (4) with the neg-entropy  $P(\mathbf{f}) = \sum_{i=1}^K f_i \ln f_i$ , the Newton method for solving the  $K$ -dim. nonlinear equation  $\partial\Lambda(\mathbf{f})/\partial\mathbf{f} = \mathbf{0}$  requires the inverse of a  $K$ -dim. Jacobian matrix for every iteration. The SMW formula makes it possible to obtain this inverse by an  $M$ -dim. matrix inversion, which leads to great computational facility whenever the number of data is much smaller than the number of unknowns, i.e.  $M \ll K$ . Additionally, for the optimization of  $\gamma$  in MEM, one may take interest in an approximated GCV of the form either  $GCV_1(\gamma) = \hat{\varepsilon}^2 / [1 - (1/M)\text{Tr}A]^2$  or  $GCV_2(\gamma) = (1/M)\|(A-I)\mathbf{g}\|^2 / [1 - (1/M)\text{Tr}A]^2$  with an approximated influence matrix  $A$  and the identity matrix  $I$ . In this application,  $GCV_2(\gamma)$  was preferable as had been in the HXT image reconstruction [8, 9]. Simulations showed that the  $\gamma$  values selected for the minimum of GCV in both the TP method and MEM were nearly optimal for recovering the original images and smaller than those selected by the Morozov condition. In MEM, a problem of reliability remained in the recovery of the value of  $GCV_2(\gamma)$ , as implied by the shot no. result in Fig. 7, as  $\gamma$  approached zero in excess of the optimal value.

Finally, for a variation of data, the performance of the Hopfield neural network was good and gave sufficiently stable reconstruction. Two examples, where the detector outputs were very different, are exhibited in Fig. 8. Here, it is seen that the outputs of the 21st detector are nearly zero and that the artifact near the horizontal camera still appears with good fitting to data as far as the data of this shot are in this region or by giving them large negative biases in the

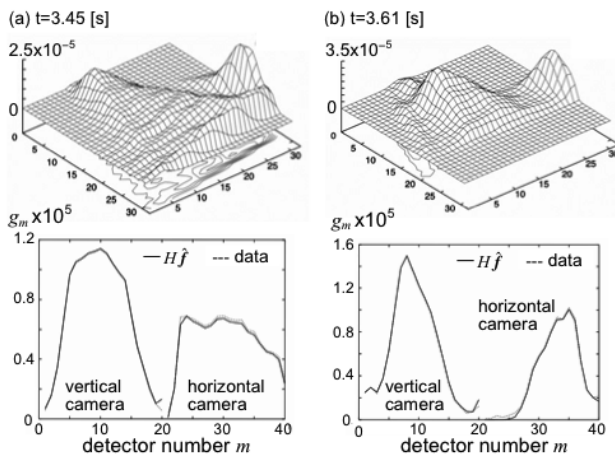


Fig. 8 Image reconstruction results of the Hopfield method in a diminishing phase of plasma: (a)  $t=3.45$  s and (b)  $t=3.61$  s in LHD shot no 31721.

concerned. Artifact elimination either by omitting neurons Hopfield iteration lead rather to the separation of  $H\hat{f}$  from  $\mathbf{g}$ . Also, no appreciable effect of artifact elimination could be obtained by the modification of minimum Fisher information type with  $P(\mathbf{f}) = \|D^{1/2}\mathbf{C}\mathbf{f}\|^2$  [6]. The modification was done in the present Hopfield neural network by practically adopting the  $\mathbf{f}^{(n)}$ -dependent weight matrix of  $W = -(2/M)(H^T H + M\gamma\mathbf{C}^T D^{(n)}\mathbf{C})$  with the diagonal matrix  $D^{(n)} = \text{diag}[(f_1^{(n)})^{-1}, (f_2^{(n)})^{-1}, \dots, (f_K^{(n)})^{-1}]$ .

#### 4. Conclusion

The Hopfield neural network works well for the bolometer tomography of LHD plasma. Based on the TP regularization with the Laplacian operator, the Hopfield model with a nonlinear activation function leads to a success of obtaining the image reconstruction of plasma both with TP-like smooth profiles and with the MEM-like positive value guarantee. Using the activation function of skimmer type leads to avoiding the saturation of plasma image and facilitates the parameter appropriation for the rapid convergence of iteration. Coding with CCS/CRS formats for sparse matrices contributes to the decrease of computing time effectively. For selecting the regularization parameter of TP type, the L-curve has proved useful. This improvement of plasma imaging requires a loss of computing time: the Hopfield iteration took about 90 s for 1,500 iterations while the fast algorithm of MEM took only about 2 s for 8 iterations, with an Ultra-Sparc-Iie 500 MHz computer.

#### Acknowledgements

The authors would like to thank Prof. T. Takeda of the University of Electro-Communication for a useful advice on the usage of the skimmer function.

- [1] J.J. Hopfield, Proc. Natl. Acad. Sci. USA **81**, 3088 (1984).
- [2] T. Okamura *et al.*, Trans. IEICE **J74-D-II**, 1661 (1991).
- [3] Y. Liu *et al.*, Rev. Sci. Instrum. **74**, 2312 (2003).
- [4] B.J. Peterson, A.Yu. Kostrioukov, N. Ashikawa *et al.*, Plasma Phys. Control. Fusion **45**, 1167 (2003).
- [5] Y. Liu *et al.*, Rev. Sci. Instrum. **77**, 10F501 (2006).
- [6] Y. Liu *et al.*, Plasma Fusion Res. **2**, S1124-1 (2007).
- [7] N. Iwama, *Phenomena in Ionized Gases*, edited by K.H. Becker *et al.* (AIP Press, New York, 1996) p. 289.
- [8] Y. Hosoda, K. Kitahashi, N. Iwama *et al.*, Proc. 24th ICPIG, Nagoya, 2001, vol. 4, p. 213.
- [9] N. Iwama, H. Hosoda, K. Kitahashi *et al.*, Bulletin of the Daido Inst. of Tech. **41**, 105 (2005).
- [10] X.F. Ma, M. Fukuhara, and T. Takeda, Nucl. Instrum. Meth. Phys. Res. **A449**, 366 (2000).
- [11] R. Barrett *et al.*, *Templates for the solution of Linear Systems: Building Blocks for Iterative Methods* (SIAM, Philadelphia, 1994).
- [12] P.C. Hansen, Inverse Problems **8**, 849 (1992).
- [13] G.H. Golub, M. Heath, and G. Wahba, Technometrics **21**, 215 (1979).